JOURNAL OF COMPUTATIONAL PHYSICS 16, 221–239 (1974)

ADI Solution of Free Convection in a Variable Viscosity Fluid*

M. H. HOUSTON, JR.† AND J. CL. DE BREMAECKER

Department of Geology, Rice University, Houston, Texas 77001

Received December 31, 1973

A numerical model of steady-state, two-dimensional free convection within an internally heated fluid of variable viscosity has been developed primarily for application to the earth's upper mantle. The dimensionless free-convection energy and stream function equations include advection, the adiabatic gradient, viscous dissipation, radiogenic heat sources, boundary heat fluxes, variable diffusivity, and variable viscosity. Both the energy equation and the fourth-order stream function equation are solved numerically by alternating direction implicit (ADI) algorithms on a special nonuniform grid first suggested by Samarskii.

The Reynolds number is negligibly small, the Rayleigh number exceeds 10^6, and the Prandtl number exceeds 10^{23}. The numerical convergence, accuracy and reliability of the method are established by various numerical tests.

1. INTRODUCTION

Ever since the pioneering experiments of Bénard [1] most studies of free convection have assumed that the convection is driven by a constant temperature differential between horizontal upper and lower boundaries; the viscosity has generally been taken as constant. Convection in the earth's mantle differs from these assumptions in several important respects:

(1) Only the upper boundary temperature is known, and much of the heat is generally believed to be due to distributed radiactive sources. This case has been little studied [2–5] and the results of the various investigations do not agree.

(2) The viscosity varies with temperature and depth. The marginal stability case for a fluid with depth-dependent viscosity has been studied in some cases [6–9], but the case of temperature- and depth-dependent viscosity appears analytically insoluble.

* Contribution # 52 of the Marine Science Institute, Geophysics Laboratory, University of Texas, Galveston, Texas.

† Now at Department of Geology, Rutgers University, New Brunswick, New Jersey.

(3) Finally, both the Prandl number and the Rayleigh number are extremely large (greater than 10^{23} and 10^6, respectively) while the Reynolds number is negligibly small; there are no experimental data on such phenomena.

Because of the preceding considerations we decided to make a numerical study of free convection under the following assumptions:

(a) rectangular two-dimensional enclosure with horizontal top and bottom,

(b) fluid with variable Newtonian viscosity,

(c) uniformly distributed heat sources,

(d) specified heat flow through the bottom,

(e) inclusion of viscous dissipation and adiabatic gradient.

The results and their geological implications are discussed in a companion paper [10]; the present paper deals with the mathematical methods.

2. Free Convection Equations

The Hydrodynamic Equations

We will assume the Boussinesq approximation, a Newtonian but variable viscosity and negligible momentum advection ("slow flow" conditions). With these assumptions the equations for mass, momentum, and energy conservation are, respectively,

$$\frac{\partial u_q}{\partial x_q} = 0, \tag{2.1}$$

$$\frac{\partial u_s}{\partial t} = -\frac{1}{\rho_0}\frac{\partial p}{\partial x_s} + \delta_{s2} g\beta T u_2 + \frac{\partial}{\partial x_q}\left[\nu\left(\frac{\partial u_s}{\partial x_q} + \frac{\partial u_q}{\partial x_s}\right)\right], \tag{2.2}$$

$$\frac{\partial}{\partial t}(CT) + u_q\frac{\partial}{\partial x_q}(CT) - u_2\frac{\partial}{\partial x_2}(\beta g T) = \frac{\partial}{\partial x_q}\left(\frac{k}{\rho_0}\frac{\partial T}{\partial x_q}\right) + H + \frac{\varphi}{\rho_0}. \tag{2.3}$$

Several methods have been devised to solve the above set of equations. The first one is to use directly the "primitive" variables (u, v, p). The MAC method [11] is the premier example of this type of solution.

Most authors [12–14] have utilized the vorticity-stream function approach. In this second method the pressure is eliminated by cross-differentiating the momentum equations. This yields two Poisson equations: one for the vorticity transport and one for the stream function. If the viscosity is constant these equations are separable.

We use a third method, which appears more suitable for variable viscosity

problems [15]. In this approach the pressure is eliminated by cross-differentiating the momentum equations, and the stream function derivatives are substituted for the velocities. This results in a fourth-order equation in the stream function Ψ, the so-called "generalized biharmonic equation."

In addition we reduce the equations to dimensionless form by application of appropriate scaling quantities. In particular,

$$x_s = \hat{x}_s/\hat{x}_{0s}\,, \qquad u_s = \hat{u}_s/\hat{u}_0\,, \qquad \theta = \hat{T}/\hat{T}_0\,, \qquad k = \hat{k}/\hat{k}_0\,,$$
$$t = \hat{t}/\hat{t}_0\,, \qquad \mu = \hat{\mu}/\hat{\mu}_0\,, \tag{2.4}$$

where "hatted" variables indicate dimensional quantities. It is convenient to use the diffusivity κ_0, and the vertical scaling length x_{02}, to form a scaling velocity and time, i.e.,

$$u_0 = \kappa_0/x_{02}\,, \qquad t_0 = x_{02}^2/\kappa_0\,. \tag{2.5}$$

The scaling factor for the stream function is $\Psi_0 = \kappa_0$.

The Dimensionless Equations

Using the previous assumptions and defining the velocities as $u = \partial\Psi/\partial y$ and $v = -\partial\Psi/\partial x$, we can write the energy equation (2.3) as

$$\frac{\partial\theta}{\partial t} + u\left(\frac{x_{02}}{x_{01}}\frac{\partial\theta}{\partial x}\right) + v\left(\frac{\partial\theta}{\partial y} - \frac{\beta g x_{02}\theta}{C}\right)$$
$$= \left(\frac{x_{02}}{x_{01}}\right)^2 \frac{\partial}{\partial x}\left(k\frac{\partial\theta}{\partial x}\right) + \frac{\partial}{\partial y}\left(k\frac{\partial\theta}{\partial y}\right) + \frac{H_0 x_{02}^2}{\kappa_0 C T_0} H + \frac{2\nu_0\kappa_0}{C T_0 x_{02}^2}\mu\left[\left(\frac{x_{02}}{x_{01}}\frac{\partial u}{\partial x}\right)^2\right.$$
$$\left. + \frac{1}{2}\left(\frac{x_{02}}{x_{01}}\frac{\partial v}{\partial x}\right)^2 + \frac{1}{2}\left(\frac{\partial u}{\partial y}\right)^2 + \left(\frac{\partial v}{\partial y}\right)^2 + \left(\frac{x_{02}}{x_{01}}\frac{\partial v}{\partial x}\right)\left(\frac{\partial u}{\partial y}\right)\right]. \tag{2.6}$$

The momentum equation (2.2) similarly becomes

$$\left[\frac{\partial^2}{\partial y^2} - \left(\frac{x_{02}}{x_{01}}\right)^2\frac{\partial^2}{\partial x^2}\right]\left\{\mu\left[\frac{\partial^2\psi}{\partial y^2} - \left(\frac{x_{02}}{x_{01}}\right)^2\frac{\partial^2\psi}{\partial x^2}\right]\right\}$$
$$+ \left(\frac{x_{02}}{x_{01}}\right)\frac{\partial^2}{\partial x\,\partial y}\left[4\mu\left(\frac{x_{02}}{x_{01}}\right)\frac{\partial^2\psi}{\partial x\,\partial y}\right] = \frac{g\beta T_0 x_{02}^3}{\kappa_0\nu_0}\left(\frac{x_{02}}{x_{01}}\right)\frac{\partial\theta}{\partial x}\,. \tag{2.7}$$

Boundary Conditions

The two-dimensional energy and stream function equations are solved within a rectangular enclosure.

Thermal boundary conditions. The sides of the enclosure are reflection surfaces with zero horizontal derivative of the temperature. The top is held at 0°C. The heat flux through the bottom is specified.

Velocity boundary conditions. The sides are reflection surfaces with the horizontal derivative of the vertical velocity equal to zero, i.e., a surface of "free slip." The horizontal velocity is zero on the sides. The top surface is also a surface of free slip with no vertical displacement allowed. At the top surface the vertical derivative of horizontal velocity is zero, and the vertical velocity is also zero. The bottom boundary is a surface of "no slip," that is, all velocities are zero along the bottom.

Stream function boundary conditions. The boundary conditions on the stream function are easily obtained from the previous boundary conditions on the velocities:

$$\text{at the bottom} \quad \partial\Psi/\partial x = \partial\Psi/\partial y = 0, \tag{2.8}$$

$$\text{at the top} \quad \partial\Psi/\partial x = \partial^2\Psi/\partial y^2 = 0, \tag{2.9}$$

$$\text{at the sides} \quad \partial\Psi/\partial y = \partial^2\Psi/\partial x^2 = 0. \tag{2.10}$$

In addition, in order for Ψ to be unique in the enclosure we must specify its value on the boundary; we choose

$$\Psi = 0. \tag{2.11}$$

3. Numerical Solution of the Partial Differential Equations

The Variable Mesh System

We choose the x-axis positive eastward. We choose the y-axis positive *downward.* The finite difference mesh has equal horizontal intervals; its vertical intervals are related by the equation

$$h_j = h_{j-1}(1 + h_{j-1}).$$

As first remarked by Samarskii [16, p. 149] this insures second-order accuracy for finite difference approximations to first- and second-order derivatives. The method has recently be rediscovered [17]. Its advantage is that it yields a higher resolution near the top where higher gradients of temperature are expected to occur.

The placement of the variables on the grid is similar to the one used in the MAC method [11]; it is shown in Fig. 1. Note that our indexing of the variables

differs slightly from that of the MAC method, e.g. our $\Psi_{i+1,j+1}$ would be $\Psi_{i+1/2,j+1/2}$ in the MAC notation. This grid scheme is attractive for several reasons. First, the velocities are easily approximated to $O(\Delta x^2)$ by central differences in Ψ, and second, advection of heat can be approximated by heat energy advected by mass flux through the four sides of the control volume. $\theta_{i,j}$ is then interpreted as the "average" temperature of the material volume centered at the position of $\theta_{i,j}$.

In order to simplify the computations, one extra node is added outside and beyond the original boundary. The sides, top and bottom of the enclosure are defined by the Ψ-nodes. Figure 2 illustrates the indexing conventions used, for the case $M = 3$, $N = 2$, which we call a 3×2 grid.

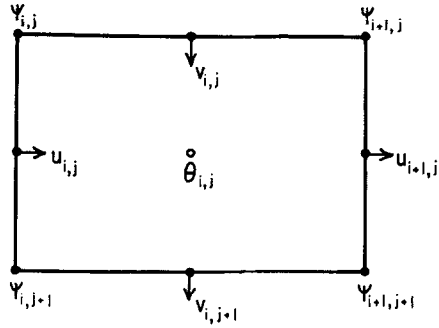

FIG. 1. Map of the relative spatial positions of θ, Ψ, u and v.

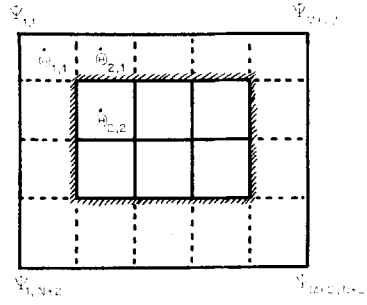

FIG. 2. Numbering convention for the Ψ grid.

Solution of the Energy Equation

The heat conduction equation can be solved by numerous methods [18–20] but the solution of the complete heat transfer equation with an advection term, is more difficult [21–23]. In the present case, however, where we are seeking a steady-state solution, these difficulties are much less serious. Furthermore, in

order to insure stability of the solution regardless of the time-step, we use upwind differencing of the temperatures. This may be written in conservative form for the x-direction as [24, 25]

$$u\,\nabla_x\theta_{i,j} = (1/2l)[\theta_{i,j}(u_{i+1,j} + |\,u_{i+1,j}\,| - u_{i,j} + |\,u_{i,j}\,|) + \theta_{i+1,j}(u_{i+1,j} - |\,u_{i+1,j}\,|) - \theta_{i-1,j}(u_{i,j} + |\,u_{i,j}\,|)].$$

We solve the energy equation by using the alternating direction implicit (ADI) method [26]. This method may be written as a two-pass procedure: A row pass, implicit in x and which yields the temperatures at time-step $n + 1/2$, and a column pass, implicit in y which yields the temperatures at time-step $n + 1$, i.e.,

$$\tfrac{1}{2}\delta_x(\theta^{n+1/2} + \theta^n) + \delta_y\theta^n = \Phi^n + (\theta^{n+1/2} - \theta^n)/\Delta t^n, \tag{3.1a}$$

$$\tfrac{1}{2}\delta_x(\theta^{n+1/2} + \theta^n) + \tfrac{1}{2}\delta_y(\theta^{n+1} + \theta^n) = \Phi^n + (\theta^{n+1} - \theta^n)/\Delta t^n, \tag{3.1b}$$

or on rearrangement,

$$(\delta_x - (2/\Delta t^n))\,\theta^{n+1/2} = -(\delta_x + 2\delta_y + 2/\Delta t^n)\,\theta^n - 2\Phi^n, \tag{3.2a}$$

$$(\delta_y - (2/\Delta t^n))\,\theta^{n+1} = \delta_y\theta^n - (2/\Delta t^n)\,\theta^{n+1/2}, \tag{3.2b}$$

where

$$\delta_x\theta^n_{i,j} = [\nabla_x(k\nabla_x) - u\nabla_x]\,\theta^n_{i,j}\,, \tag{3.3a}$$

$$\delta_y\theta^n_{i,j} = [\nabla_y(k\nabla_y) - v\nabla_y]\,\theta^n_{i,j}\,, \tag{3.3b}$$

and Φ^n includes the terms of internal heat generation and viscous dissipation:

$$\Phi^n_{i,j} = H_{i,j} + \varphi^n_{i,j}\,,$$

$H_{i,j}$ = internal heat generation at temperature node $\theta_{i,j}$,

$\varphi^n_{i,j}$ = viscous dissipation at temperature node $\theta_{i,j}$,

$$\varphi^n_{i,j} = 2\mu^n_{i,j}\left[\left(\frac{\partial u_{i+1/2,j}}{\partial x}\right)^2 + \left(\frac{\partial v_{i,j+1/2}}{\partial y}\right)^2 + \frac{1}{2}\left(\frac{\partial u_{i+1/2,j}}{\partial y}\right)^2 + \frac{1}{2}\left(\frac{\partial v_{i,j+1/2}}{\partial x}\right)^2 + \left(\frac{\partial u_{i+1/2,j}}{\partial y}\right)\left(\frac{\partial v_{i,j+1/2}}{\partial x}\right)\right],$$

where

$$u_{i+1/2,j} = \tfrac{1}{2}(u_{i,j} + u_{i+1,j}),$$

$$v_{i,j+1/2} = \tfrac{1}{2}(v_{i,j} + v_{i,j+1}).$$

The boundary conditions can be very simply written using the extra node outside the enclosure, and taking into account the variable vertical spacing.

Note that the boundaries do not pass through the θ nodes (Fig. 2). At the upper boundary, for example, where the temperature $\theta^n_{i,ub}$ is specified,

$$\theta^n_{i,1} = \theta^n_{i,ub} - (h_1/2)(\partial\theta^n/\partial y)]_{ub}$$

or

$$\theta^n_{i,1} = [(h_1 + h_2)/h_1]\,\theta^n_{i,ub} - (h_1/h_2)\,\theta^n_{i,2}\,, \tag{3.4}$$

which yields $\theta^n_{i,1}$. Other boundary conditions can be derived by similar procedures.

Solution of the Momentum Equation

The momentum equation (2.2) has been written as a generalized biharmonic equation (2.7). We solve it by an extension of the ADI method of Conte and Dames [27, 28]. These authors devised a method for solving the ordinary biharmonic equation in a square region with mixed boundary conditions. They proved convergence and provided a near optimum choice for the iteration parameters. Their two step iteration scheme can be written

$$\Psi^{n+1/2}_{i,j} = \Psi^n_{i,j} - r^n(\nabla_y{}^4\Psi^{n+1/2}_{i,j} + 2\nabla_y{}^2\nabla_x{}^2\Psi^n_{i,j} + \nabla_x{}^4\Psi^n_{i,j} - h^4 f_{i,j}), \tag{3.5}$$

$$\Psi^{n+1}_{i,j} = \Psi^{n+1/2}_{i,j} - r^n(\nabla_x{}^4\Psi^{n+1}_{i,j} - \nabla_x{}^4\Psi^n_{i,j}), \tag{3.6}$$

where r^n is a positive iteration parameter chosen so as to speed convergence, and where $\nabla_y{}^4$ is the finite difference approximation to $h^4\,\partial^4/\partial y^4$ with similar definitions for $\nabla_x{}^2\nabla_y{}^2$ and $\nabla_x{}^4$.

We have adapted Conte and Dames' scheme to variable viscosity by replacing the biharmonic form with constant coefficients by a variable viscosity version. In addition, at Dr. Rachford's suggestion, the acceleration parameter was made inversely proportional to the average local viscosity.

In our notation, $\nabla_y{}^4$ is the finite difference approximation to $\partial^4/\partial y^4$, $\nabla_x{}^2\nabla_y{}^2$ to $\partial^4/\partial x^2\,\partial y^2$, etc. This difference from Conte and Dames accounts for the minor differences in the equations. In our case, $r^n_{i,j}$ also contains a normalizing factor proportional to $l^{-2}h_j^{-1}h_{j-1}^{-1}$.

We thus obtain

$$\Psi^{n+1/2}_{i,j} = \Psi^n_{i,j} - r^n_{i,j}[\nabla_y{}^2(\mu^n_{i,j}\nabla_y{}^2\Psi^{n+1/2}_{i,j}) - \nabla_y{}^2(\mu^n_{i,j}\nabla_x{}^2\Psi^n_{i,j})$$
$$- \nabla_x{}^2(\mu^n_{i,j}\nabla_y{}^2\Psi^n_{i,j}) + 4\nabla^2_{xy}(\mu^n_{i,j}\nabla^2_{xy}\Psi^n_{i,j}) + \nabla_x{}^2(\mu^n_{i,j}\nabla_x{}^2\Psi^n_{i,j}) - f_{i,j}], \tag{3.7}$$

$$\Psi^{n+1}_{i,j} = \Psi^{n+1/2}_{i,j} - r^n_{i,j}[\nabla_x{}^2(\mu^n_{i,j}\nabla_x{}^2\Psi^{n+1}_{i,j}) - \nabla_x{}^2(\mu^n_{i,j}\nabla_x{}^2\Psi^n_{i,j})]. \tag{3.8}$$

In the equation above, $f_{i,j}$ is the driving function for the stream function equation and is equal to the Rayleigh number, R_a, times the horizontal derivative of temperature at the point $\Psi^n_{i,j}$ (see Eq. (2.7)).

Application of the above algorithm involves the solution of a pentadiagonal matrix that is symmetric for constant viscosity and nearly symmetric for variable viscosity.

The boundary conditions are, again, written very simply. At the top ($j = 2$), for example $\partial^2\Psi/\partial y^2 = 0$ (see Eq. (2.10)), thus

$$(\Psi^n_{i,j+1}/h_j(h_{j+1} + h_j) - (\Psi^n_{i,j}/h_j h_{j+1}) + (\Psi^n_{i,j-1}/h_j(h_{j+1} + h_j)) = 0,$$

but $\Psi^n_{i,2} = 0$ (see Eq. 2.11); hence we obtain

$$\Psi^n_{i,1} = -h_2\Psi^n_{i,3}/h_3\,. \tag{3.9}$$

Other boundary conditions are easily derived.

Steady-State Solutions

To minimize the cost of machine computations and maximize the utility of the model, we have chosen to obtain steady-state solutions before attempting time-dependent ones. This enables us directly to compare steady-state solutions resulting from models with different parameters, e.g. convection driven entirely by boundary heat flux or entirely by internal heat sources. Such a comparison enhances our understanding of the roles of the various parameters. In order to accomplish this the energy equation is still solved as if it were time-dependent, but time is now treated not as an independent variable, but as an iteration parameter chosen to accelerate convergence [29]. A "global" iteration consists of a pass through both the temperature and stream function solutions, together with an update of the dependent variables (viscosity, conductivity). Furthermore, it was found best to restrict Δt to some value proportional to

$$1/\{||u_{i,j}/\Delta x\,|_{\text{Max}}\,,\,|\,v_{i,j}/\Delta y_j\,|_{\text{Max}}\,|_{\text{Max}}\}. \tag{3.10}$$

This is equivalent to restricting the value of the smallest Courant number within the solution grid [20, p. 40]. Particular values of Δt were selected by experimentation.

Although there is some justification for viewing sequential iterations as a steady-state solution or similar to actual time-dependent solutions [30] we emphasize that here Δt, strictly speaking, is an "acceleration" parameter. We have limited experience with a true time-dependent solution. However, preliminary experiments indicated stable and reasonable solutions were computed using a Δt ten times the value suggested in Eq. (3.10).

Although the method so far described does not diverge, it oscillates around the steady-state solution: The variation of Ψ_{Max} is approximately $\pm 10\,\%$. These oscillations are probably due to phase distortion [31]. In order to avoid this

problem the driving function, $f_{i,j}$, is taken as the average of its values before and after each global iteration. With such averaging, the oscillations in the constant viscosity cases are less than 0.1 % and less than 1 % in all other cases.

Fromm [32] has reported that no phase induced instabilities resulted if "new" temperatures were used in the buoyancy terms. However, in our case, we found that use of the "new" temperatures caused oscillation. Averaging the "new" and "old" temperatures in the buoyancy term for the stream function greatly reduced the amplitude of the oscillations.

Convergence Criteria

The iteration convergence of the energy equation is defined by a root mean square change (RMSC)

$$\text{RMSC} = \left[\left(\sum_i \sum_j (\theta_{i,j}^{n+1} - \theta_{i,j}^{n})^2\right) \Big/ \sum_i \sum_j (\theta_{i,j}^{n})^2\right]^{1/2},$$

where n denotes the sequence number of double iterations. The iterations are continued until RMSC $< \epsilon$ ($\epsilon = 10^{-5}$) or until $n > N$, where N is usually 50.

The iteration convergence of the stream function equation is similar but $\epsilon = 2 \cdot 10^{-6}$ and $N = 160$. Usually less than 50 double iterations bring the stream function equation to a "converged" status. As a further precaution the relative change between successive solutions is required to be less than $5 \cdot 10^{-3}$ at all computation nodes.

Global convergence of the overall scheme is a judgment based on the constancy from iteration to iteration of

(a) isotherm profiles,
(b) stream function isopleths,
(c) horizontally averaged vertical temperature derivatives,
(d) surface heat flux, and
(e) mean temperature.

The computations are terminated when all the above quantities indicate an equilibrium condition in the enclosure.

4. Numerical Convergence Tests

It is necessary to carry out numerical convergence tests in order to establish the reliability of the results of the present method. Theoretical consideration of the stability and convergence of our finite difference scheme in the sense of Lax and Richtmyer [33] is difficult; hence the analytic consideration of stability was

bypassed in favor of a more pragmatic attempt to show convergence by numerical experimentation.

One can distinguish between mathematical convergence of the finite difference equations to the partial differential equations, and numerical convergence of the finite difference method of solution. Here we are speaking of the latter.

General methods for proving numerical convergence can be grouped into several categories; one may

(a) test against a known solution;
(b) attain the "same" solution starting from different initial conditions;
(c) utilize symmetry;
(d) use different mesh and "time" increments.

All the above methods have been used to establish the convergence and accuracy of our method. Though a definitive proof of the numerical solution is lacking (i.e., direct comparison with a physical experiment), the accumulated "indirect" evidence for convergence, as detailed below, argues strongly for the reliability of the presented solutions.

The Energy Equation

It is well known that upwind differencing results in a stable *explicit* equation [18, pp. 397–399; 25]. Roache [20] quotes Pearson [34] as having shown that the ADI method is stable when central differences are used. However, the error eigenfunctions used by Pearson [34, p. A-32] are real only when the advection terms are smaller than the conduction terms; otherwise they are imaginary. This proof thus lacks generality.

The difficulty of proving the convergence of ADI methods, as well as the power of these methods, is well-recognized [35, 36]. Even in the simpler case where the matrices H and V (corresponding, respectively, to a row and column pass) are symmetric but noncommutative, the proof is difficult [36], in the present case, where neither H nor V is symmetric, a rigorous proof of convergence has not been established. Instead the finite difference approximations of the individual terms in the energy equation were carefully monitored for their effects on a time-dependent temperature solution. Using symmetry, a variety of simple initial conditions, and both finer and coarser nets, confidence in the ADI temperature solution was established. In addition, the close similarity between our solutions and those of McKenzie *et al.* [4, 5] reinforces this confidence.

The Stream Function Equation

Conte and Dames [27, 28] have established the convergence of the ADI method as applied to the biharmonic equation with constant coefficients; because of the

TABLE I

Parameters of the Models

	CGS or other units	SI units
Depth	$7 \cdot 10^7 = 700$ km	$7 \cdot 10^5$
Width	$1.96 \cdot 10^8 \cong 2000$ km $3.0 \cdot 10^8 = 3000$ km	$1.96 \cdot 10^6$ $3.0 \cdot 10^6$
Density, ρ_0	3.5 g/cm^3	$3.5 \cdot 10^3$
Specific heat, C	$1.3 \cdot 10^7$ erg/g °C	$1.3 \cdot 10^3$
Thermal expansivity, β	$3.7 \cdot 10^{-5}$/°C	$3.7 \cdot 10^{-5}$
Thermal conductivity, k_0	$1.1 \cdot 10^{-2}$ cal/cm °C sec	4.6
Kinematic viscosity, ν_0	$5 \cdot 10^{21}$ cm^2/sec	$5 \cdot 10^{17}$
Radiogenic heating,[a] H	$1.9 \cdot 10^{-7}$ erg/g sec	$6.7 \cdot 10^{-8}$ W/m^3
Heat flux through bottom	0.3 HFU	$1.25 \cdot 10^{-2}$

[a] Distributed over the depth of the cell, this corresponds to a surface heat flow of 1.1 HFU $= 4.6 \cdot 10^{-2}$ SI units.

variable viscosity in the present case, their analysis is not applicable. However, using our formulation we have reproduced the published results of Conte and Dames [28, p. 271] for a clamped and a simply supported plate under a uniform load, by setting all viscosities (equivalent to "plate stiffness") and mesh intervals constant. At the point of maximum deflection the two solutions agree to within 10^{-4}.

The accuracy of the variable mesh scheme vs constant mesh in the solution of the fourth-order stream function equation was evaluated by a series of tests with constant viscosity. The values of the parameters used in this and all subsequent tests are shown in Table 1.

A temperature anomaly in the form of a 0 to π cosine wave was impressed upon a field of constant temperature within a 9×9, 15×15, and 20×20 grid. Using this temperature field as a driving function, the stream function equation was solved with both variable and constant vertical mesh intervals. As shown in Fig. 3, the differences among the solutions are small.

Convergence Tests of the Numerical Convective Solution

Though each of the ADI solutions for the temperature and stream function may separately be convergent, we must still establish convergence for the combined system of equations. A first series of numerical experiments was run with constant viscosity, internal radioactive heating equivalent to 1.11 HFU, and bottom flux

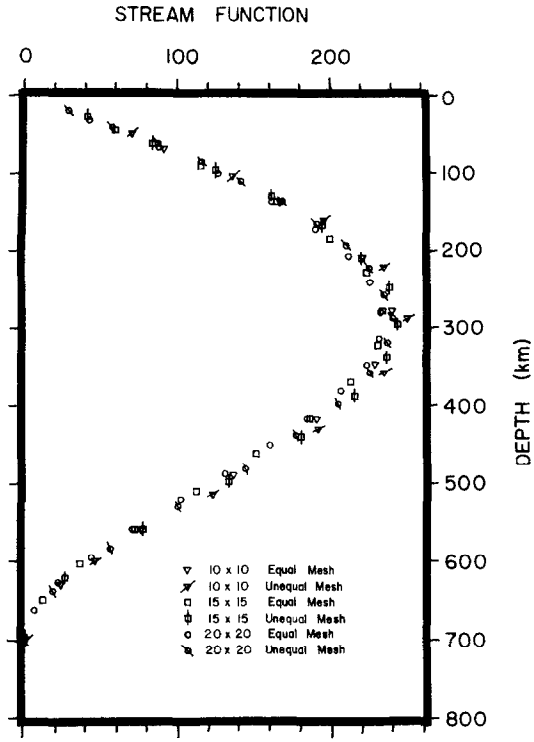

FIG. 3. Stream function profiles from ADI stream function convergence test with constant viscosity.

of 0.3 HFU for variable grids of 9×9, 15×15, and 20×20. The aspect ratio of the cell was chosen so that two symmetric cells should develop within the enclosure [31]; the cell height is 700 km, the width is 2000 km. Figures 4–6 illustrate the final "converged" isotherms and isopleths for each of the three grids. These lines are drawn as linear interpolations between adjacent computation nodes.

The similarity among all three solutions is apparent. As expected, the coarsest grid shows the greatest deviation. Moreover, all the solutions show a high degree of symmetry which argues for the accuracy of the solution. In addition, several solutions which were initiated with slightly different temperature anomalies converged to the same solution.

A more detailed comparison shows that the average temperature on the 9×9, 15×15 and 20×20 grids are, respectively, 551, 504 and 506°C; the largest temperature difference between the last two grids is less than 20°C. Similarly the stream function maxima are, respectively, 87, 81 and 79. Finally, the average

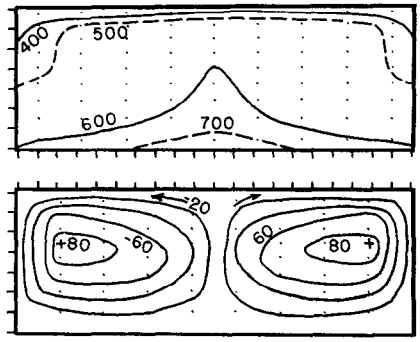

FIG. 4. Convergence test with constant viscosity on a 9 × 9 grid: bottom, normalized stream function; top, temperature in °C.

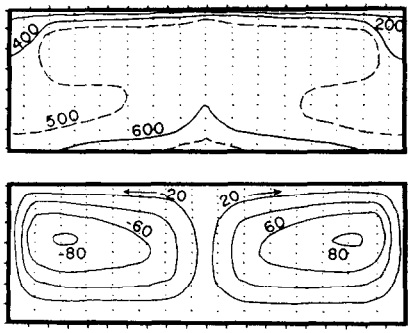

FIG. 5. Convergence test with constant viscosity on a 15 × 15 grid: bottom, normalized stream function; top, temperature in °C.

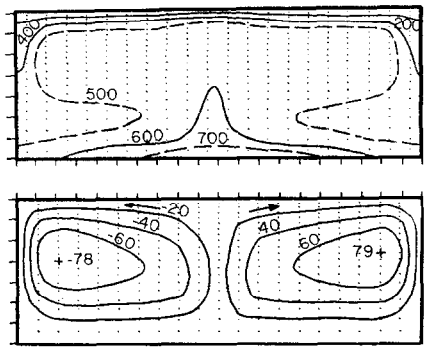

FIG. 6. Convergence test with constant viscosity on a 20 × 20 grid: bottom, normalized stream function; top, temperature in °C.

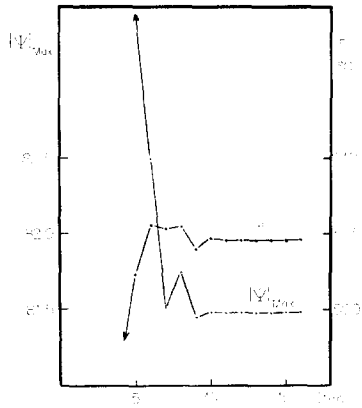

FIG. 7. Variation in $|\Psi|_{max}$ and in the average temperature of the cell for the 15 × 15 constant viscosity case vs the iteration number.

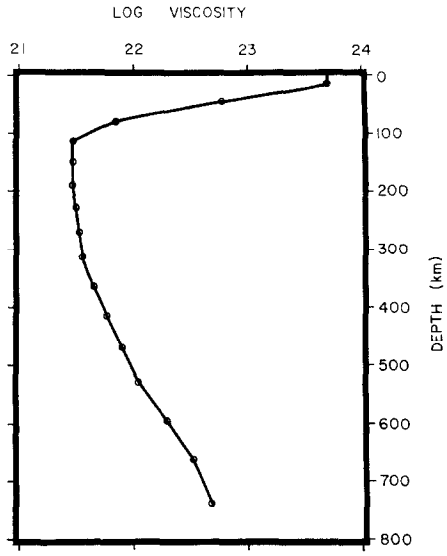

FIG. 8. Variable viscosity profile used in Fig. 9 and 10. The circles show the values used in the 15 × 15 solution.

heat flux at the surface are, respectively, 1.37, 1.35 and 1.33 HFU, which is within 6% of the theoretical value of 1.41 HFU.

A final line of evidence is provided by Fig. 7 which shows the convergence of the stream function maximum and the average temperature of the cell towards their final values; the absence of oscillations is noteworthy. The average heat flow at the surface fluctuates even less.

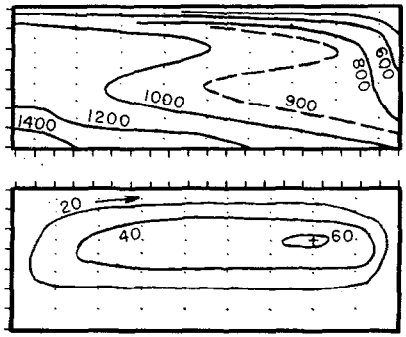

FIG. 9. Convergence test with variable viscosity on a 9 × 9 grid: bottom, normalized stream function; top, temperature in °C.

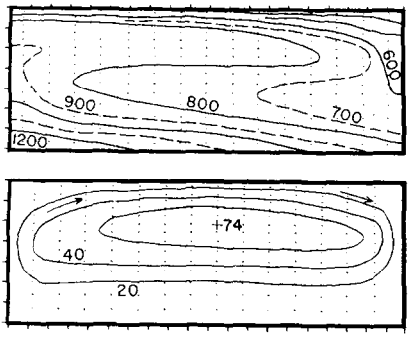

FIG. 10. Convergence test with variable viscosity on a 15 × 15 grid: bottom, normalized stream function; top, temperature in °C.

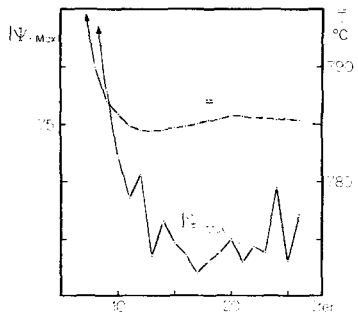

FIG. 11. Variation in $|\Psi|_{max}$ and in the average temperature of the cell for the 15 × 15 variable viscosity case vs the iteration number.

The above evidence strongly implies that the results obtained on a 15×15 grid are within a very few percent of the exact results.

It is of some interest to note that, for symmetry to develop on a very coarse grid (e.g. 9×9), there should be an odd number of temperature grid points in the x-direction. This allows the midpoint to be a maximum and favors symmetry; if such condition is not fulfilled, departures from symmetry are to be expected. On the other hand, as the 20×20 net demonstrates, this condition is not important on a reasonably fine net.

Experiments were also conducted with a viscosity depending only on depth; the viscosity profile used is shown in Fig. 8. All other parameters are as given in Table 1. Note that the viscosity varies by a factor of more than 100 over less than 1/7 of the depth of the enclosure. The results of the computations using 9×9 and 15×15 grids are shown in Figs. 9 and 10. The two solutions are quite similar in the general aspects of the circulation and the temperature fields. For the latter however, the 9×9 solution is about 200°C hotter than the 15×15 solution, while the stream function maxima differ by about 20%. (They differed by 10% in the constant viscosity case.) Considering that the high viscosity region near the surface is represented by a single point in the 9×9 solution, these differences are not surprising.

It may be noted that the average heat flow at the surface in the 15×15 case is 1.40 HFU, and 1.36 in the 9×9 case (theoretical value 1.41 HFU), while the average temperatures are, respectively, 785° and 943°C. (This 20% difference corresponds to a 10% difference in the constant viscosity case.) Finally, Fig. 11 shows the convergence of the average temperature and of the stream function maximum toward their final values. While the variation is greater than in the constant viscosity case, still the average temperature fluctuates by less than 0.1% and the stream function maximum by less than 1%.

Conclusions

The numerical method presented solves the two-dimensional free convection equation for an internally heated fluid of variable viscosity. Both the second-order energy transport equation and the fourth-order stream function equation are solved by alternating direction implicit (ADI) methods. Though definitive proof of the numerical stability, convergence, and accuracy of the method is lacking, indirect evidence from systematic numerical tests strongly support the reliability of the model.

With due heed to the two-dimensionality of the numerical solutions, as compared to the inherent three-dimensionality of most convection phenomena, numerical modeling appears to be a powerful tool with which to explore quantitatively the

nature of free convection within a material of high but variable viscosity, such as the earth's upper mantle.

NOTATION

Greek Letters	*Definition*
β	thermal expansivity
Γ	constant determining size of Δt^n
δ_{qs}	substitution tensor
θ	dimensionless temperature
κ	coefficient of thermal diffusivity
μ	viscosity or dimensionless viscosity
ν	kinematic viscosity
ρ	density
φ	viscous dissipation function
Φ	viscous dissipation and volumetric heat sources
Ψ	stream function, usually dimensionless

Roman Letters	*Definition*
c	Courant number, $c = \Delta x/\Delta t$
C	specific heat
g	acceleration of gravity
H	radiogenic heating
h_j	jth vertical increment in Ψ-mesh
i	index in x-direction
j	index in y-direction
k	thermal conductivity
l	horizontal space increment in the Ψ-mesh
p	pressure
q	index; = 1, 2
$r^n_{i,j}$	acceleration parameter in nth ADI solution at position Ψ_{ij}
s	index; = 1, 2
t	time
Δt^n	nth pseudotime interval
T	temperature
u	velocity in the x-direction
v	velocity in the y-direction
x	coordinate variable in horizontal direction, positive eastward
x_{0s}	scaling length in s-direction
y	coordinate variable in the vertical direction, positive downward

Symbols	*Definition*
$O(h)$	first order in h
∇x	finite difference derivatives in x-direction
∇y	finite difference derivatives in y-direction
δ_x	second-order finite-difference derivative including advection in the x-direction
δ_y	second-order finite-difference derivative including advection in the y-direction

Notes. (1) A subscript of 0 (as in ρ_0) denotes a reference quantity or a dimensional scaling parameter. (2) The summation convention is to be used only on index q.

ACKNOWLEDGMENTS

The help of Professor H. H. Rachford, Mathematics Department, Rice University, is gratefully acknowledged. We also thank the anonymous referee who suggested averaging the driving function, and the Marine Science Institute, Geophysics Laboratory, University of Texas, Galveston, Texas for the grant of computer time. Acknowledgment is made to the donors of the Petroleum Research Fund administered by the American Chemical Society for the major support of this research. One of us (M.H.H.) was supported by the National Defense Education Act during this period.

REFERENCES

1. H. BÉNARD, *Ann. Chim. Phys.* **23** (1901), 62–144.
2. P. H. ROBERTS, *J. Fluid Mech.* **30** (1967), 33–49.
3. D. J. TRITTON AND M. N. ZARRAGA, *J. Fluid Mech.* **30** (1967), 21–31.
4. D. P. MCKENZIE, J. M. ROBERTS, AND N. O. WEISS, *Tectonophys.* **19** (1973), 89–103.
5. D. P. MCKENZIE, J. M. ROBERTS, AND N. O. WEISS, *J. Fluid Mech.* **62** (1974), 465–538.
6. C. P. MCFADDEN AND D. E. SMYLIE, *Nature (London)* **220** (1968), 468–469.
7. C. P. MCFADDEN, The effect of a region of low viscosity on thermal convection in the Earth's Mantle, Unpublished thesis, Univ. of Western Ontario, London, Ontario, Canada, 1969.
8. T. D. FOSTER, *J. Geophys. Res.* **74** (1969), 685–693.
9. H. TAKEUCHI AND S. SAKATA, *J. Geophys. Res.* **75** (1970), 921–927.
10. M. H. HOUSTON, JR. AND J.-CL. DE BREMAECKER, Numerical models of convection in the upper mantle, *J. Geophys. Res.*, in press.
11. F. H. HARLOW AND J. E. WELCH, *Phys. Fluids* **8** (1965), 2182–2183.
12. K. E. TORRANCE AND D. L. TURCOTTE, *J. Fluid Mech.* **47** (1971), 113–125.
13. K. E. TORRANCE AND D. L. TURCOTTE, *J. Geophys. Res.* **76** (1971), 1154–1161.
14. F. M. RICHTER, *Rev. Geophys. Space Phys.* **11** (1973), 233–287.
15. D. J. ANDREWS, *J. Geophys. Res.* **77** (1972), 6470–6481.
16. V. K. SAUL'YEV, "Integration of Equations of Parabolic Type by the Method of Nets" (English Translation), MacMillan, New York, 1964.
17. H. SUNDQVIST AND G. VERONIS, *Tellus* **22** (1970), 26–31.

18. G. E. FORSYTHE AND W. R. WASOW, "Finite-Difference Methods for Partial Differential Equations," Wiley, New York, 1960.
19. R. S. VARGA, "Matrix Iterative Analysis," Prentice-Hall, Englewood Cliffs, NJ, 1962.
20. P. J. ROACHE, "Computational Fluid Dynamics," Hermosa, Albuquerque, NM, 1972.
21. H. L. STONE AND P. L. T. BRIAN, *A.I.Ch.E. J.* **9** (1963), 681–688.
22. M. NOBLE, R. THOMPSON, AND M. M. WELLS, *EOS, Trans. Am. Geophys. U.* **54** (1973), 309.
23. A. O. GARDER, JR., D. W. PEACEMAN, AND A. L. POZZI, *J. Soc. Pet. Eng.* **4** (1964), 26–36.
24. A. D. RUNCHAL, D. B. SPALDING, AND M. WOLFSHTEIN, *Phys. Fluids, Suppl.* **2** (1969), 21–28.
25. D. L. TURCOTTE, K. E. TORRANCE, AND A. T. HSUI, Convection in the earth's mantle, *in* "Methods in Computational Physics" (B. A. Bolt, Ed.), Vol. 13, pp. 431–454, Academic Press, N.Y., 1973.
26. J. DOUGLAS, JR. AND H. H. RACHFORD, JR., *Trans. Amer. Math. Soc.* **82** (1956), 421–439.
27. S. D. CONTE AND R. T. DAMES, *Math. Tables Aid Comput.* **12** (1958), 198–205.
28. S. D. CONTE AND R. T. DAMES, *J. Assoc. Comput. Mach.* **7** (1960), 264–273.
29. D. W. PEACEMAN AND H. H. RACHFORD, JR., *J. Soc. Ind. Appl. Math.* **3** (1955), 28–41.
30. P. R. GARABEDIAN, *Math. Tables Aids Comput.* **10** (1956), 183–186.
31. J. E. FROMM, *Phys. Fluids* **8** (1965), 1757–1769.
32. J. E. FROMM, *IBM J. Res. Develop.* **15** (1971), 186–196.
33. P. D. LAX AND R. D. RICHTMEYER, *Comm. Pure Appl. Math.* **9** (1956), 267–293.
34. C. E. PEARSON, "A computational method for time-dependent two-dimensional incompressible flow problems," Sperry Rand Res. Report SRRC-RR-64-17, 1964.
35. O. B. WIDLUND, *IBM J. Res. Develop.* **11** (1967), 239–243.
36. O. B. WIDLUND, *Math. Comp.* **20** (1966), 500–515.